Artificial Intelligence-Based Hierarchical Control Design for Current Sharing and Voltage Restoration in DC Microgrid of the More Electric Aircraft

Habibu Hussaini, *Student Member, IEEE*, Tao Yang, *Senior Member, IEEE*, Ge Bai, *Student Member, IEEE*, Matías Urrutia-Ortiz, *Student Member, IEEE*, and Serhiy Bozhko, *Senior Member, IEEE*

***Abstract*— In the conventional droop control method employed in the primary control layer, there is an inherent trade-off between current-sharing accuracy and voltage regulation. Consequently, to achieve both accurate current sharing and maintain the bus voltage at its nominal value, secondary control schemes are implemented. Nevertheless, a proper design of control parameters of an electrical power system (EPS) is important as it has a huge impact on its stability and dynamic features. To that end, this paper proposes a novel artificial intelligent-based design strategy for the optimal design of the power sharing and bus voltage compensation coefficients for the islanded more electric aircraft (MEA) EPS DC microgrid. Through the proposed approach, the bus voltage regulation and dynamic performance of the MEA EPS are improved in different EPS operation conditions when compared with the state-of-art methods. Furthermore, the safety and continuous operation of the electrical loads onboard the MEA are guaranteed. The proposed control approach can be conveniently implemented since there is no need for additional controllers and existing communication infrastructure such as power line communication can be utilized. The effectiveness of the proposed approach is validated in both simulations and hardware-in-the-loop experiments.**

***Index Terms*—Artificial intelligence, droop control, optimal droop gains, fault tolerance, more electric aircraft**

I. Introduction

THE more electric aircraft (MEA) electrical power system (EPS) distribution network used as a case study in this paper is a typical DC microgrid (MG) operating in the islanding mode. The DC MG has advantages such as no harmonics concerns, easier to control, and better power quality, reliability, and efficiency when compared with AC MG [1]. A typical configuration for the future MEA EPS is made up of multiple parallel-connected sources interfaced with their respective converters and linked to a common DC bus via transmission cables [2, 3]. Fig. 1 depicts the connection of two electrical generators (i.e., permanent magnet synchronous generators (PMSGs) to separate engine shafts: a high-pressure (HP) shaft and a low-pressure (LP) shaft. Alongside the generators, an auxiliary power unit (APU) is also present in the aircraft, serving as a backup power source in the event of engine or generator failure. The generators operate in parallel, collectively supplying power to the DC bus. In aerospace applications, permanent magnet generators (PMGs) are favoured over other electrical machines such as switched reluctance starter/generators (SRSGs), wound-field synchronous machines (WFSMs), or induction generators (IG). This preference is attributed to the advantages in power density, volume, and weight [4]. Furthermore, achieving controlled power sharing among the generators holds the potential to decrease the required generator capacity and enable operation at maximum efficiency levels [4]. Also, in such a configuration, the EPS can provide continuous power to the loads in a situation whereby one of the sources fails. However, a major concern in

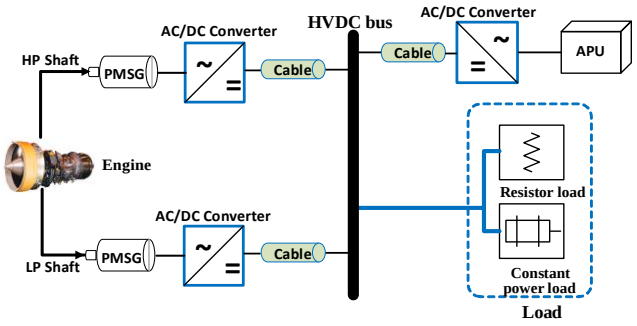

Fig. 1 Single-bus HVDC distribution network utilized in the MEA EPS [4]

This work was supported by the Clean Sky 2 Joint Undertaking through the European Union's Horizon 2020 Research and Innovation Programme under Grant 737814. The author Habibu Hussaini also thanks the stipend funding from Petroleum Technology Development Fund (PTDF), Nigeria. (*Corresponding author: Tao Yang*.)

Habibu Hussaini is with the Power Electronics, Machines and Control Group, University of Nottingham, Nottingham NG7 2RD, U.K, and with the Department of Electrical and Electronics Engineering, Federal University of Technology, Minna, P.M.B. 65, 920101, Minna, Niger, Nigeria. (email: Habibu.Hussaini@nottingham.ac.uk, habufarid@futminna.edu.ng).

Tao Yang, Ge Bai, and Serhiy Bozhko are with the Power Electronics, Machines and Control Group, The University of Nottingham, Nottingham NG7 2RD, U.K. (emails: Tao.Yang@nottingham.ac.uk; Ge.Bai@nottingham.ac.uk, Serhiy.Bozhko@nottingham.ac.uk).

Matías Urrutia, is with print Electric Limited, Peregrine House, Ford Lane, West Sussex, BN18 0DF, UK. (email: matias.urrutia@sprint-electric.com)

such a system operating in the islanded mode is the problem of power sharing and bus voltage regulation [5] which if not properly handled may result in power quality and stability issues in the EPS. In addition, the EPS could experience a huge disturbance when there is a sudden load change or one of the sources is under fault conditions. This disturbance may cause a significant drop in the bus voltage which can be harmful to loads, incur additional losses, affect the power quality and make the EPS less stable. In this regard, there is a need for a robust control technique that will guarantee stable operation in different conditions of the EPS by restricting the bus voltage variation within an acceptable range while enhancing the current sharing dynamic performance. These are crucial issues that need to be addressed and are the focus of this paper. Besides, a safety-critical application [6] such as the MEA requires a great control performance over the bus voltage in most conditions of the aircraft operations to power the electrical loads onboard and to meet MIL-STD-704F [7] and DO-160E [8] voltage standards.

Though there are different control strategies (such as master/slave control), droop control has been widely employed in DC systems for power sharing among parallel sources and converters, due to its reliability, simplicity, modularity, ease of control and independence from a digital communication network technology [5, 9]. However, the unequal distribution line resistance and offset in the nominal voltage reference are the two main practical factors that affect the performance of the droop control method. Furthermore, there is an inherent tradeoff between current-sharing accuracy and bus voltage regulation in the traditional droop control method [10].

The most suitable control strategy to tackle such concerns to realize both bus voltage compensation and improved load sharing simultaneously is the implementation of a secondary control [9, 11]. The secondary control level is used for voltage restoration due to the deviations generated by the primary control. The secondary control scheme is categorized into centralized, distributed and decentralized control schemes. A detailed review of each of these secondary control schemes can be found in [11]. The distributed control scheme is the most commonly used secondary control scheme and is regarded as a tradeoff between centralized and decentralized control schemes. In this control method [12, 13, 14, 15, 16, 17, 18, 19, 20, 21], the secondary control is implemented in local controllers that share information among themselves through a low bandwidth digital communication (LBC) link, without depending on a central controller. The use of large droop gains is recommended in [12, 13, 19, 20, 21] to minimize the error in load sharing at the primary control level which is due to the potential inequality in nominal voltages and feeder resistance. Consequently, in [12], the product of the average current calculated by each local controller and a constant shift coefficient is used to shift up the droop characteristics line in each module in a proportionate manner as the load increases for compensation of the bus voltage deviation. In [15], the poor voltage regulation and load-sharing errors are compensated separately with the aid of a proportional (P) controller and a proportional-integral (PI) controller respectively. However, just as in [12], the principle of selecting the compensation coefficient is also difficult. A voltage drop of about 12% was recorded in [15] and to almost zero in [20] when one of the sources was disconnected due to being under a faulty condition. Hence, their bus voltage regulation performance during the transient period can be regarded as poor. In [22, 23], adaptive droop control algorithms with secondary controllers to suppress the circulating current and the effect of line resistance on current sharing in a low-voltage DC microgrid are proposed. In these proposed methods, the droop parameters of the converters are adaptively adjusted following the estimated line resistance of the corresponding subsystem. However, their control performance is highly dependent on the accurate estimation of the feeder resistance. Moreover, since the distributed secondary control relies on a digital communication link, the availability, expandability and reliability of the whole system will reduce. This will also increase the cost of the system and possibly its weight [24]. In addition, it may suffer from communication latency, traffic and cyber-attacks [25, 26], which are not desirable in a safety-critical application such as the MEA EPS.

To improve the system's reliability, a decentralized secondary control scheme that is independent of a communication link is proposed in [27, 28, 29, 30, 31]. In [27], a proportional (P) controller is implemented at the secondary control level to mitigate the influence of distribution line resistance on load sharing. The proposed control method relies only on the local controllers and all the control variables are measured locally. Although independent of a communication link, however, it requires accurate knowledge of the line resistance to determine the gain of the P-controller to adjust the droop gain of each converter module for better load sharing and DC bus voltage regulation. Besides, it is difficult to estimate the line resistance in practical situations. Also, its bus voltage regulation performance is poor under heavy load conditions and a source outage. The secondary control approaches presented thus far for voltage restoration rely either on online parameter estimation, communication medium and/or an extra PI controller [12]-[30]. Hence, making the control system complex and unreliable.

In sharp contrast to the conventional voltage compensation methods, an improved bus voltage compensation approach to eliminate the deviation of the bus voltage and improve power sharing performance is proposed in [31]. In the proposed method, the droop gains of the converters are set to be larger than the cable resistance to achieve accurate power sharing at the primary control level. Compared with existing approaches, although the approach in [31] has the advantage of not requiring a digital communication link and extra controllers, it can only provide good bus voltage regulation performance when the participating converters are contributing to the load current. Therefore, making the voltage regulation performance depends on the EPS condition.

Despite the good progress made in previous secondary control methods, high droop gains are commonly set for the converters to achieve accurate power sharing at the primary control level. It is observed that this makes the control system less robust and reliable in the event of a source fault and/or

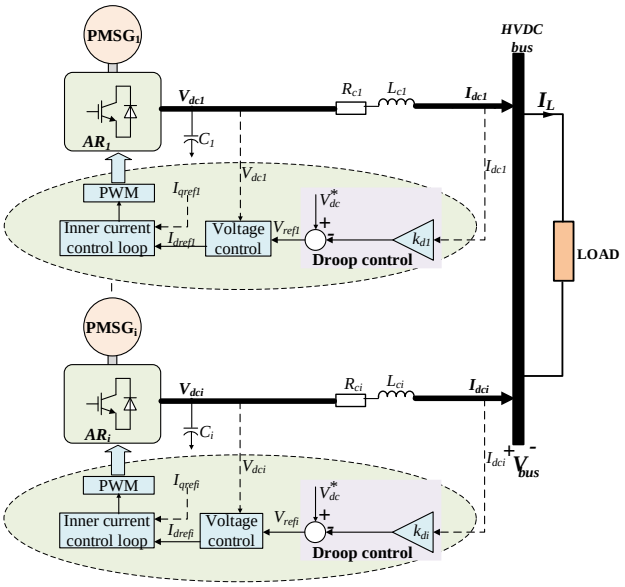

Fig. 2 Typical 270 V Single bus Multi-source HVDC architecture for future MEA EPS architecture with decentralized power sharing method

failure of the secondary control. This is of great concern and makes it crucial for further investigation into the design of the control parameters. It is expected that by the optimal design of the control parameters, the EPS should be able to maintain operation with good bus voltage performance in different conditions of the EPS. A safety-critical application such as the MEA EPS could benefit from such an optimal design.

Motivated by the challenges enumerated above, this paper focuses on the optimal design of the control parameters used for power sharing and bus voltage compensation at the primary and secondary control levels respectively by developing a novel artificial intelligence-based design methodology. The proposed optimal design of the droop and bus voltage compensation coefficients is to maintain a good power quality within an acceptable range and ensure robust control performance during load changes, source failure and even in a situation of the failure of the secondary control. The main contribution of this article is the development of a new neural network-based design strategy for the computation of the optimal droop and compensation coefficients based on desired power sharing ratio and bus voltage regulation. Also, because the design process is entirely performed offline, no computational burden is incurred on the system during implementation. Detailed simulation and hardware-in-the-loop experimental results validate the effectiveness and performance of the proposed control approach in terms of robust performance in different EPS operation conditions. Furthermore, a comparative assessment of the proposed approach with the control method used in [31] shows that the proposed method performs well in terms of power sharing and bus voltage regulation under a source outage even when the compensation coefficient is not updated and in the event of the failure of the secondary control.

The rest of the paper is organized as follows. The description of the architecture of the system under study, its droop control analysis and the proposed bus voltage compensation method are presented in section II. The proposed artificial intelligence-

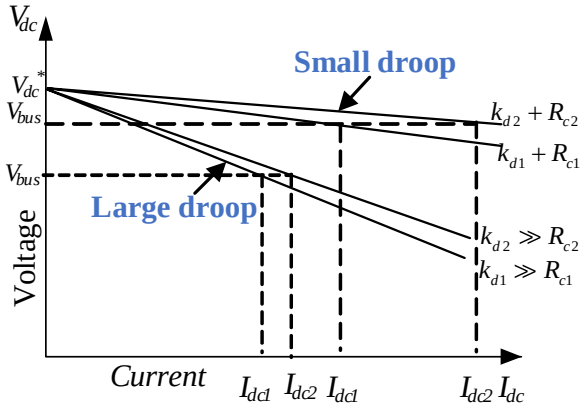

Fig. 3 The *V-I* characteristics for unequal load sharing due to the influence of unequal line resistances in the system

based control parameters design for power sharing and bus compensation coefficients is described in Section III. Section IV presents simulation results to validate the proposed control and design strategies, including a comparison with an existing control approach. The experimental results and conclusion of the paper are discussed in Sections V and VI respectively.

II. System Architecture and Control

A. Description of the System Architecture and Control Structure

This paper considers the MEA EPS 270 V HVDC distribution network architecture with three parallel connected generators, i.e. permanent magnet synchronous generators $PMSG_1$-$PMSG_3$, which are driven by two engine shafts and the auxiliary power unit (APU) respectively. These generators are feeding power to a common DC bus through their dedicated AC-DC converters (denoted as $AR_1 \ldots AR_i$) as shown in Fig. 2. The generation systems, each with one PMSG and one AC/DC converter (referred to as *PMSG-AR* system), are connected to the DC bus with cables represented by resistive-inductive models. Within this MEA EPS, *PMSGs* extract power from aircraft engines or APUs. The electrical loads (mainly resistive and constant power loads (CPLs) are supplied from the DC bus. Power sharing among the *PMSG-AR* systems is traditionally accomplished using the droop control method.

The next section will provide an overview of the droop control method and discuss its limitations. Thereafter, a control design strategy to achieve both accurate current sharing and bus voltage compensation will be presented.

B. Analysis of the primary droop control mechanism

The droop control method being a primary level control is implemented on each of the *PMSG-AR* systems as shown in Fig. 2. It is worthy of note that, for well-designed voltage and current loops, the output voltage V_{dci} of each of the parallel-connected converters should track its reference voltage V_{refi} (i.e., $V_{refi} = V_{dci}$). Therefore, for proper power sharing, the relationship between the local DC voltage obtained from the droop control function (shown in Fig. 2) and the output current

of the converter is expressed as

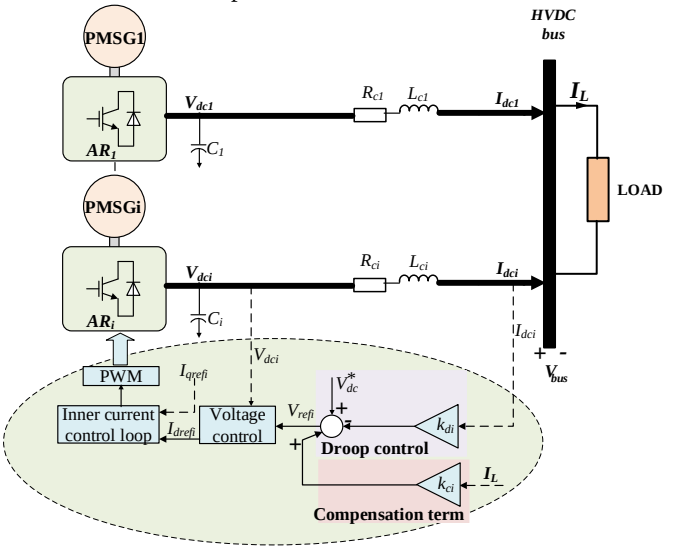

Fig. 4 Proposed Hierarchical Control scheme for the MEA EPS DC grid

$$V_{ref\,i} = V_{dc}^{*} - k_{di} I_{dci} \tag{1}$$

where i = 1,2,3 is the number of subsystems, V_{refi} is the reference local dc-link voltage corresponding to output current I_{dci}, the $V_{dc}^{*}$is the nominal DC voltage (270 V), I_{dci} is the measured output current of the converter, and k_{di} is the virtual resistance or droop gain of the converter.

By considering only the distribution line resistance R_{ci} (the line inductance L_{ci} can be ignored since it does not affect the system's steady-state performance), the bus voltage V_{bus} is computed as $V_{bus} = V_{dci} - R_{ci}I_{dci}$ (as shown in Fig. 2). Thus, the bus voltage can be expressed as

$$V_{bus} = V_{refi} - R_{ci} I_{dci} = V_{dc}^{*} - (k_{di} + R_{ci}) I_{dci} \tag{2}$$

From (2), it can be derived that

$$(k_{di} + R_{ci}) I_{dci} = (k_{dj} + R_{cj}) I_{dcj} \quad \forall i, j = 1,.....,N \tag{3}$$

Therefore, from (3), it can be deduced that the current sharing ratio between the converters is inversely proportional to the sum of the designed droop gain k_{di} and distribution line resistance R_{ci}. Hence, they will both influence the power sharing ratio.

Consequently, from (3) and for the three *PMSG-AR* systems considered in this paper, the current sharing ratio between the converters (with converter 1 taken as the base value) can be computed as

$$n_1 = \frac{I_{dc2}}{I_{dc1}} = \frac{k_{d1} + R_{c1}}{k_{d2} + R_{c2}} \tag{4}$$

$$n_2 = \frac{I_{dc3}}{I_{dc1}} = \frac{k_{d1} + R_{c1}}{k_{d3} + R_{c3}} \tag{5}$$

where n_1 and n_2 are the current sharing ratio between converter 1 and 2, and converter 1 and 3 respectively.

In the conventional droop gain design, the droop gain parameter is usually limited and determined based on the power rating of the converters to ensure that the bus voltage regulation is low and maintained within an acceptable range using the expression in (6).

$$k_{di} \le \frac{\delta V_{\max}}{I_{dci\max}} \tag{6}$$

where I_{dcimax} is the maximum/full-load output current of the ith converter and the maximum allowable deviation of the DC bus voltage is δV_{max}. The value of δV_{max} is usually set to be about 5% of the nominal voltage V_{dc}^{*} [32]. In addition, the same droop gains are traditionally set for the converters when the sources have equal ratings. However, from (4) and (5), it can be observed that when the droop gain set for the converters is small, identical and comparable to the unequal line resistance R_{ci}, the error in current sharing (i.e., $I_{dc1} - I_{dc2}$) will be significantly high as shown in Fig. 3.

Conversely, to solve the problem of inaccurate current sharing, the straightforward approach is to set a sufficiently high droop gain larger than the line resistance (i.e., $k_{di} \gg R_{ci}$) for the converters. This way the influence of the unequal line resistance on current sharing will be largely mitigated (i.e., $I_{dc1} - I_{dc2}$ will reduce). However, the major drawback of this approach is that with a large droop gain set for the converters, the bus voltage regulation becomes very poor (as shown in Fig. 3) and may be unacceptable to loads for many practical applications. Additionally, the system stability and power quality will be threatened [15]. The result of either of the above two choices (i.e., using the conventional droop gain design or selecting large droop gain for the converters) is demonstrated using the *V-I* droop characteristics curve shown in Fig. 3 for a two-converter system. Therefore, based on the identified challenges associated with the selection of the droop gain at the primary control level as shown in Fig. 3, a better solution will be to optimize the droop gain. It is expected that the optimal droop gain should be able to mitigate the influence of the unequal line resistance on the droop control to yield accurate power sharing and good bus voltage regulation at the primary control level.

However, it can be observed from (2) that due to the droop control, the bus voltage V_{bus} will not be equal to its nominal value V_{dc}^{*}, except if I_{dci} = 0. Moreover, the deviation will be more pronounced when a fault occurs on one of the generators and is disconnected from the system and under load changes. Therefore, there is a need to compensate for the bus voltage deviation and maintain it at or near its nominal value.

C. Proposed bus voltage compensation

One way to maintain the DC bus voltage at its nominal value is by adjusting the converter references. Hence, this paper proposes the bus voltage restoration using a feedforward compensation technique as shown in Fig. 4. In the proposed technique, a secondary compensation term ΔV is designed and added as feedforward into the primary controller (shown in Fig. 2) as

$$V_{ref\,i} = V_{dc}^{*} - k_{di} I_{dci} + \Delta V \tag{7}$$

thus, the HVDC bus voltage V_{bus} after compensation becomes

$$V_{bus} = V_{dc}^{*} - (k_{di} + R_{ci}) I_{dci} + \Delta V \tag{8}$$

It can be observed from (7), that the droop characteristics can be shifted (i.e., adjusted) along the voltage axis by adding a correction term ΔV. As the ultimate control goal is to achieve V_{bus} to be 270V, thus the total load current on the HVDC bus is critical and is used in the compensation term as

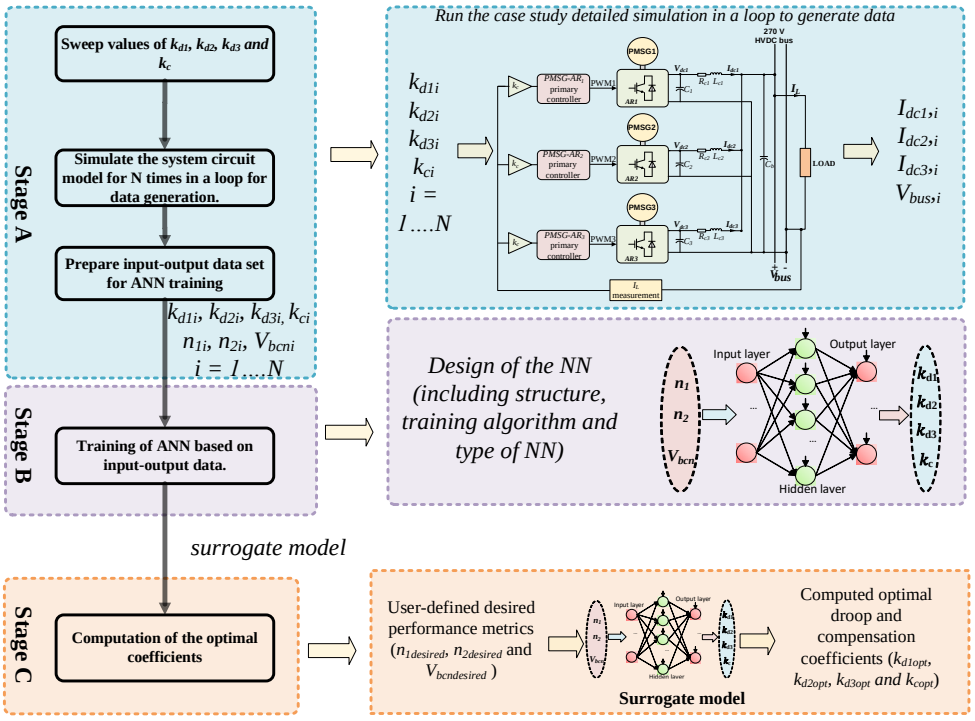

Fig. 5 Flowchart for the design of the droop and compensation coefficients using ANN approach

$$\Delta V = k_c I_L \tag{9}$$

where the total load current I_L is given as

$$I_L = I_{dc1} + I_{dc2} + I_{dc3} = (V_{dc}^* - V_{bus}) \sum_{i=1}^{n} \frac{1}{(k_{di} + R_{ci})} \tag{10}$$

From (9) and (10), we can see that the voltage reference of each power source in the system can be adjusted using the compensation term via a feedforward link as shown in Fig. 4. As shown in Fig. 4, each local dc-link voltage reference V_{refi} (i=1,2,3) is now added with a common compensation term ΔV associated with the total load currents (i.e. $k_c I_L$). No extra communication link or voltage controller is needed. The total load current I_L is transmitted to the local controllers via power line communication [11]. To achieve expected compensation and power sharing, the coefficient k_c and local droop k_{di} need to be properly selected and will be discussed in Section III.

To facilitate the development of our proposed optimal control parameters design and computation strategy in Section III, the way the droop and compensation coefficients are selected in [31] will be presented first since the feedforward technique is also used for the voltage compensation. In the first instance, the individual droop gains k_{di} are selected for the converters to be larger than the line resistance R_{ci} (i.e., $k_{di} \gg R_{ci}$) to mitigate the effect of cable resistance on power sharing. Also, the voltage compensation coefficient referred to as the global droop gain k_c is selected as follows. From (10), the droop characteristics of the DC bus are defined by the expression in (11) [31]

$$k_c = \frac{1}{\sum_{i=1}^{n} \frac{1}{(k_{di} + R_{ci})}} \tag{11}$$

where k_c is the global droop gain. By selecting the individual droop gain to be large, the effect of line resistance in (11) can be ignored. Hence, the expression in (11) can be re-written as

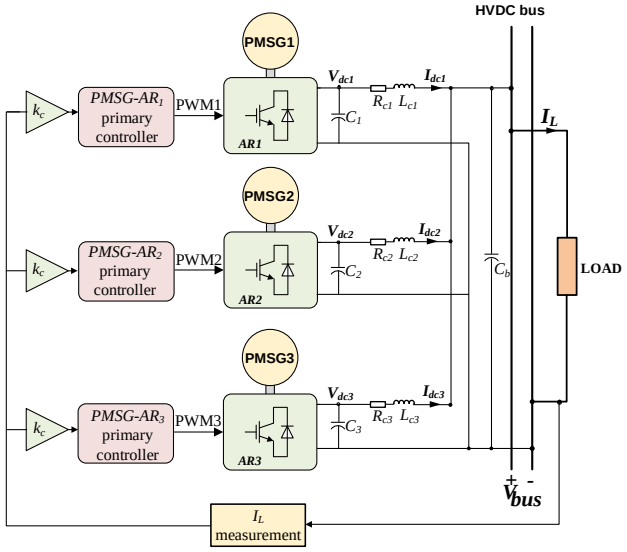

Fig. 6 Case study setup

$$k_c = \frac{1}{\sum_{i=1}^{n} \frac{1}{k_{di}}} \tag{12}$$

It can be observed from (12) that the global droop gain k_c is closely related to the individual high droop gains k_{di}. This coefficients selection process has the following drawbacks.

i. In a situation where not all the participating converters are contributing to the load current due to for example a source failure, then, the bus voltage regulation becomes poor [17]. To solve this problem and restore the bus voltage to its nominal value, the global droop gain will need to be updated in real-time according to the new EPS condition. Thus,

TABLE I Simulation Input Variables Ranges for Data Generation

Parameter	Range	Sampling Step	Number of Samples
$1/k_{d1}$	[3.825, 4.675]	0.085	11 x 11 x 11 x 11 = 14,641
$1/k_{d2}$	[3.825, 4.675]	0.085	
$1/k_{d3}$	[3.825, 4.675]	0.085	
$1/k_c$	[11.475, 14.025]	0.255	

TABLE II Parameters of the system used as case study in simulations and experiments

Category	Parameters	Values
PMSG parameters	Nominal power	45 kW
	Base speed	8000 rpm
	Switching frequency	100 kHz
	Maximum modulation index	0.9
	Pole pair	3
	Stator winding resistance R_s	1.058 mΩ
	Winding inductance L_d=L_q	99 µH
	Flux linkage ψ_m	0.03644 Wb
Converter, cable and load parameters	DC-link capacitance C_b	0.8 mF
	Local capacitor $C_{1\text{-}3}$	1.2 mF
	Converter dead time T_d	3 µs
	DC-link bus voltage V_{bus}	270 V
	Traditional droop coefficients k_{d1}, k_{d2}, and k_{d3}	1/4.25, 1/4.25, 1/4.25
	Line resistances R_{c1}, R_{c2}, and R_{c3}	3 mΩ,30 mΩ, 15 mΩ
	Line inductances L_{c1}, L_{c2}, and L_{c3}	1 µH, 10 µH, 5 µH
	Load power used for data extraction	40 kW

requiring extra effort.

ii. If the secondary control fails and only the primary droop control is working, the high individual local droop gain selected for the converters will lead to a huge drop in the bus voltage. Such a huge drop in the bus voltage is not ideal for the electrical loads onboard the aircraft and it will degrade the system performance, causing power quality and system stability issues.

Therefore, the way the droop and compensation coefficients are selected in [31] makes the control approach highly dependent on the EPS condition and less robust. Motivated by these challenging issues, a novel and intelligent design strategy for the optimal design of the control parameters to safeguard a safety-critical application such as the MEA EPS from such vulnerabilities and ensure acceptable voltage regulations in different conditions of the EPS will be developed. The control problem is considered an optimization problem in which an ANN-based surrogate model is used for the computation of the optimal settings of the droop and compensation coefficients. A detailed comparison between our proposed approach and the method used [31] is provided in Section IV-D.

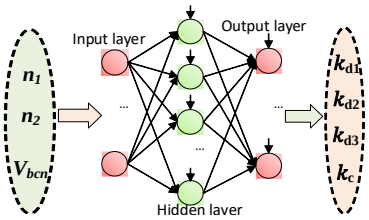

Fig. 7 Schematic of the NN-based surrogate model

III. Droop and Compensation Coefficients Design Using Artificial Neural Network

The main objective of this section is to introduce the design process of the optimal droop gain of each power source, $k_{di,}$ and compensation coefficient, k_c, to achieve accurate power sharing and bus voltage restoration. A neural network-based design strategy for the computation of the optimal droop and compensation coefficients that will yield a user-defined desired power sharing ratio and bus voltage compensation at the primary control and secondary control levels simultaneously will be developed.

A. Methodology

Fig. 5 shows the flowchart of the design steps to be followed. As shown in Fig. 5, there are three stages (i.e., stages A, B and C) in the process of obtaining the optimal control coefficients. Each of the stages is discussed as follows.

i. *Stage A: Data generation*

To generate data to train the ANN, the detailed model of the case study shown in Fig. 5 is built in MATLAB Simulink and is simulated with different combinations of the droop gains, k_{d1}, k_{d2}, and k_{d3}, and the compensation coefficient, k_c within a design space shown in TABLE I. The corresponding current sharing ratios, n_1 and n_2, and normalized bus voltage V_{bcn} = V_{bus}/270 are thus derived and stored after each simulation cycle. A total of 14,641 data samples were obtained from the simulation exercise. The multiple simulations were run in a loop with the aid of MATLAB codes on a standard computer with quad-core processors. Each simulation run costs around 6 s, thus, it costs approximately about 6 hours to generate the entire data samples. The system parameters used in the simulation for data generation are shown in TABLE II. In stage A, the relationship between the inputs (x) to the simulation model and processed outputs (y) can be represented as

$$y = F(x) \Leftrightarrow (n_1, n_2, V_{bcn}) = F(k_{d1}, k_{d2}, k_{d3}, k_c) \quad (13)$$

ii. *Stage B: Training and development of the surrogate model*

The data generated from stage A is used to train an ANN-based surrogate model in stage B. The ANN is trained with the current sharing ratios (n_1 and n_2), and the normalized bus voltage (V_{bcn}) as inputs and the droop and compensation coefficients (k_{d1}, k_{d2}, k_{d3}, and k_c) as outputs to derive a fast surrogate model to allow quick computation of the optimal control coefficients. The feedforward neural network (FFNN) structure shown in Fig. 7 with the backpropagation training algorithm is used in this paper for the training and development

of the surrogate model.

The FFNN structure is made up of 3 neurons in the input layer which are equivalent to the three system outputs n_1, n_2 and V_{bcn}, 11 neurons in the hidden layer and 4 neurons in the output layer which are equivalent to the four design variables k_{d1}, k_{d2}, k_{d3} and k_c). The surrogate model represents the input-output data mapping relationship in (14).

$$y = F(x) \Leftrightarrow (k_{d1}, k_{d2}, k_{d3}, k_c) = F(n_1, n_2, V_{bcn}) \quad (14)$$

The ANN-based surrogate model is usually employed to establish the relationship between input data and output data through mapping in situations where the relationship between the two is unknown or computationally intensive to assess. It can approximate non-linear functions to a high degree of accuracy with little knowledge about the system [33]. The training was implemented using the built-in NN fitting toolbox in MATLAB. Further details about the NN fundamental working principle, structure selection and training process can be found in [34, 35].

iii. *Stage C: Deployment of the surrogate model*

Finally, after training, the surrogate model can be used in stage C and power system designers can define the desired current sharing ratios (i.e., $n_{1desired}$ and $n_{2desired}$) and normalized bus voltage regulation ($V_{bcndesired}$) that are within the design space as input to the surrogate model to compute the optimal droop and compensation coefficients (k_{d1opt}, k_{d2opt}, k_{d3opt} and k_{copt}) to yield such control performance. The computed optimal droop and compensation coefficients can then be used to control the load sharing and bus voltage regulation as desired in both simulations and experiments.

The proposed design strategy only requires specific input-output data measurement and does not need detailed information and knowledge of the system under study. Hence, making it robust when compared with existing design approaches.

B. Design consideration and stability concerns

Before carrying out the proposed design approach, the design range of the design variables (i.e., k_{di} and k_c) should be pre-defined. It is important to choose a proper design range for the design variables in such a manner that the stability of the system will not be compromised and based on the desired control objectives. To that end, the upper and lower bounds (i.e., design range) of each of the droop gains are defined to be +10% and -10% respectively of the traditional fixed droop gains. The traditional fixed and identical droop gains are shown in TABLE II and are designed based on the conventional droop gain design using (6) as mentioned in section II-B to ensure an acceptable voltage regulation and stable operation of the EPS. Furthermore, a detailed comparative stability analysis of droop control approaches in voltage source converter-based DC microgrids carried out in [36], found that the maximum droop gain for stable operation should not exceed

$$k_{di} < \frac{V_{dc}^{*2}}{4P_{cpl}} - R_{ci} \quad (15)$$

where P_{cpl} is the power of constant power loads connected to the DC bus. Thus, by substituting the system parameters shown in TABLE II and the CPL of 40 kW used during data generation in (15), the maximum droop gain for stable operation in our case study should not exceed 0.4256. It can therefore be said that the design range selected for the droop gains (shown in TABLE I) is feasible and will not affect the stability of the MEA EPS. For the compensation coefficient k_c, its range is selected as shown in TABLE I to maintain the droop control function and guarantee system stability [12].

C. Computational burden

The data generation stage (i.e., stage A) costs time (i.e., computational burden) and this may increase exponentially with an increasing number of design variables. Quantitatively speaking, the time taken (offline) for the data generation was estimated by using the duration it costs to run one single simulation as a yardstick. Therefore, for the 14,641 design variable combinations and simulation runs, the computational burden for the data generation amounted to about 6 hours on a standard computer with quad-core processors. However, it would have only cost around 1 hour or less to run the simulations for the same design variable combinations on a computer with a 24-core processor by running the simulations in parallel with the aid of the parallel computing toolbox in MATLAB and a few lines of codes. It is important to note that, although, this stage A comes with some computational costs (offline), however, it is only required to be executed once and not for every coefficient design that is within the design space.

The training stage B is straightforward and can be accomplished quickly using the NN fitting toolbox in MATLAB. The usual challenge in this stage is the selection of a suitable number of neurons for the hidden layers. Although the selection is done using a trial and error process, the process can be executed quite fast. Besides, the NN fitting toolbox generates results quickly. Thus, the power system designer can arrive at a suitable number of neurons within a short time.

The trained surrogate model can output results with just a click of a button after being provided with appropriate inputs. Thus, making this stage several orders of magnitude faster than stages A and B.

IV. Design Examples and Validation of the Proposed Approach

A. Design examples

In this section, the trained surrogate model is used to compute the optimal droop and compensation coefficients to realize two (2) exemplary control goals for the MEA EPS. The two (2) design cases considered in this paper are explained as follows.

1) Design example 1: Equal load sharing and bus voltage compensation

In this design example, the sources ($PMSG_{1-3}$) are assumed to have equal ratings (i.e. $I_{dc1}^{rated} = I_{dc2}^{rated} = I_{dc3}^{rated}$) and thus expected to share the load current demand equally while maintaining the bus voltage regulation at its nominal value in steady states. To achieve this control performance, the desired current sharing ratios and normalized bus voltage which are used as inputs to the surrogate model are defined as $n_{1desired} = 1$, $n_{2desired} = 1$, and $V_{bcndesired} = 1$. Consequently, the computed

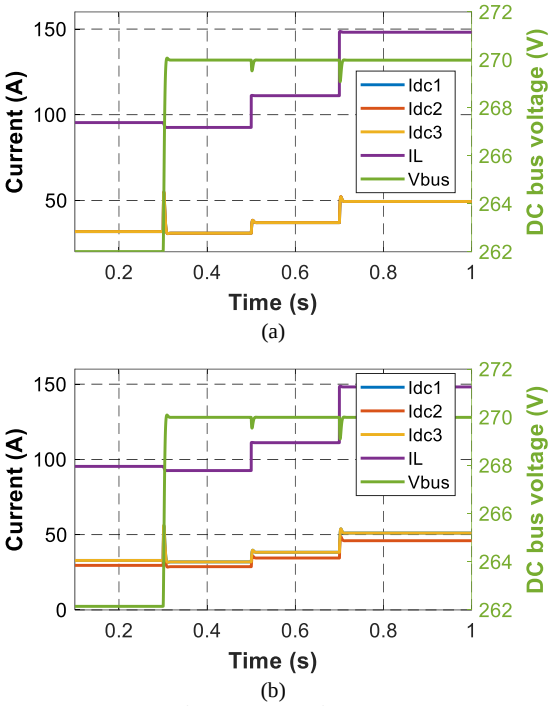

Fig. 8 Simulation results of the case study for load sharing and bus voltage regulation using (a) Optimal droop and compensation coefficient settings from design example 1 (b) Optimal droop and compensation coefficient settings from design example 2

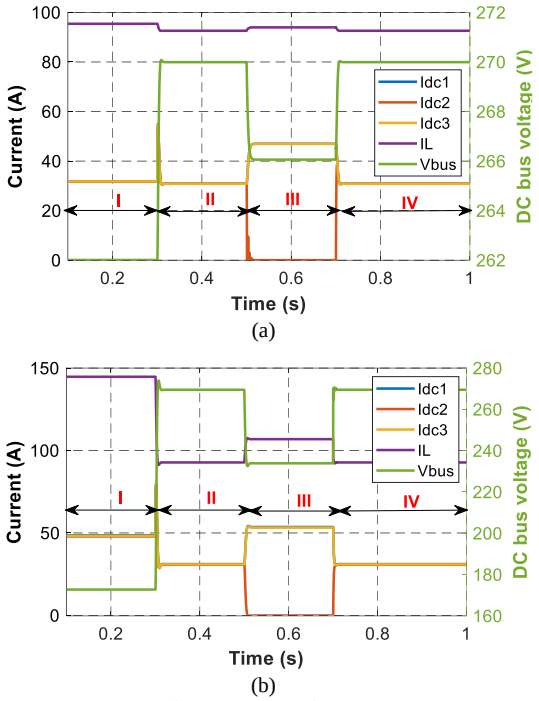

Fig. 9 Simulation results of the case study for load sharing and bus voltage regulation comparison between (a) Proposed method (b) Approach presented in [31]

optimal droop and compensation coefficients by the surrogate model are obtained as k_{d1opt} = 1/4.0305, k_{d2opt} = 1/4.5211, k_{d3opt} = 1/4.2342, and k_{copt} = 1/11.9501.

2) Design example 2: Unequal load sharing and bus voltage compensation

In this design example and within the design space considered in this paper, $PMSG_1$ and $PMSG_3$ are assumed to have equal ratings but 10 % higher than that of $PMSG_2$ (i.e. $0.9I_{dc1}^{rated}$ = I_{dc2}^{rated}= $0.9I_{dc3}^{rated}$). Therefore, $PMSG_{1,3}$ is expected to share the load demand equally and more than $PMSG_2$. In addition, the bus voltage regulation is desired to be maintained at its nominal value in steady states. To achieve this control objective, the desired current sharing ratios and normalized bus voltage which are inputs to the surrogate model are defined as $n_{1desired}$ = 0.9, $n_{2desired}$ = 1, and $V_{bcndesired}$ = 1. Thus, the computed optimal droop and compensation coefficients by the surrogate model are k_{d1opt} = 1/4.2434, k_{d2opt} = 1/4.2540, k_{d3opt} = 1/4.4698, and k_{copt} = 1/12.1502.

The validity of these computed optimal coefficients from the two design examples will be tested first in simulation and then in experiments in Section V.

B. Design Validation using Simulation

In this section, the performance of the proposed approach with the optimal control coefficient settings is validated and compared with the conventional droop control method and the approach proposed in [31] using simulation case studies. In this regard, the MEA EPS distribution network case study (shown in Fig. 6) with three *PMSG-AR* systems working in parallel is modelled in MATLAB/Simulink. The simulation parameters are the same as those shown in TABLE II.

Table III Comparison of branch current and transmission loss of the method in [31] and proposed control approach

Method		[31]	Proposed approach
Stage I	Branch currents (I_{dc1}/I_{dc2}/I_{dc3})	48.55 A /47.91 A/48.26 A	31.80 A/31.80 A/31.80 A
	Transmission loss	110.90 W	48.54 W
Stage III	Branch currents (I_{dc1}/ I_{dc2}/ I_{dc3})	53.60 A/0.00 A/53.28 A	46.98 A/0.00 A/46.98 A
	Transmission loss	51.20 W	39.73 W
Stages II and IV	Branch currents (I_{dc1}/ I_{dc2}/ I_{dc3})	31.12 A/30.71 A/30.94 A	30.86 A/30.86 A /30.86 A
	Transmission loss	45.71 W	45.56 W

1) Case 1: Normal scenario

Fig. 8 (a) and (b) show the simulation results of the case study based on using the optimal coefficient settings obtained from design examples 1 and 2 respectively. The simulation parameters are shown in Table II. CPLs of 25 kW, 30 kW and 40 kW are applied at times 0.1 s, 0.5 s and 0.7 s respectively during the simulation.

As shown in Fig. 8 (a), from time t = 0.1 s to t = 0.3 s only the primary control (i.e., droop control) is activated, hence, the bus voltage drop to around 262 V which represents a 2.96 % deviation of the bus voltage from its nominal value. This is an advantage of using the optimal droop gain settings at the primary control level. Though it cannot maintain the bus voltage at its nominal value at this control level due to the droop

TABLE IV Comparison of different voltage compensation methods

Control method	Technique employed	Voltage regulation with SC	Voltage regulation with SC and under a SO	Voltage regulation without SC	Low bandwidth communication	Additional controller	Reliability	Parameter estimation required	Complexity of implementation
Ref. [12]	Average voltage and current compensation	Good	Poor	Very poor	Yes	Yes	Low	No	Medium
Ref. [31]	Feed-forward	Good	Poor	Very poor	No	No	Medium	No	Low
Refs. [22, 23]	Droop gain adjustment	Precise	Good	Good	Yes	Yes	Medium	Yes	High
Proposed	Feed-forward	Precise	Good	Good	No	No	High	No	Low

control action, however, it can mitigate the tradeoff between the current sharing accuracy and bus voltage regulation. Besides, a voltage range of between 250 V to 280 V is acceptable for the MEA application in steady states [7]. However, immediately the secondary control is activated at t = 0.3 s, the voltage drop at the primary control level is compensated and the bus voltage is restored to its nominal value as desired (i.e., $V_{bcndesired}$ = 1). Furthermore, the bus voltage is maintained at its nominal value despite the load changes. Also, equal current sharing in the desired ratio ($n_{1desired}$ = 1 and $n_{2desired}$ = 1) is achieved at both primary and secondary control levels irrespective of the load fluctuations. The result of this case study shows that the proposed approach can guarantee both proportional current sharing and bus voltage restoration simultaneously as desired.

Similarly, as shown in Fig. 8 (b), from t = 0.1 s to t = 0.3 s only the primary control is activated, hence, the bus voltage drop to around 262.15 V which represents a 2.91 % deviation of the bus voltage from its nominal value. However, immediately the secondary control is activated at t = 0.3 s, the voltage drop at the primary control level is compensated and the bus voltage is restored to its nominal value as desired (i.e., $V_{bcndesired}$ = 1). Furthermore, the bus voltage is maintained at its nominal value despite the load changes. Also, proportional current sharing in the desired ratio ($n_{1desired}$ = 0.9 and $n_{2desired}$ = 1) is achieved at both primary and secondary control levels irrespective of the load changes. This result demonstrates that the proposed approach can yield proportional current sharing and bus voltage restoration simultaneously as desired.

2) Case 2: Comparison with an existing method

Here, the proposed control approach is compared with the one presented in [31]. The control parameters for our proposed method are k_{d1opt} = 1/4.0305, k_{d2opt} = 1/4.5211, k_{d3opt} = 1/4.2342, and k_{copt} = 1/11.9501 as obtained from design example 1. The parameters for [31] are $k_{d1} = k_{d2} = k_{d3}$ = 2, and k_c = 2/3 to meet the condition $k_{di} \gg R_{ci}$. The simulation parameters are the same as in Case 1. The system goes through the following four stages:

Stage I (0.1 – 0.3 s): A CPL of 25 kW is applied in the simulation and only the primary control (i.e. droop control is activated) at t = 0.1 s;

Stage II (0.3 – 0.5 s): Secondary control is implemented at t = 0.3 s;

Stage III (0.5 – 0.7 s): PMSG-AR$_2$ is disconnected from the system (assumed to be under fault condition);

Stage IV (0.7 – 1 s): The fault is cleared and the *PMSG-AR$_2$* is re-connected back to the system.

The simulation result for this case study is shown in Fig. 9 (a) and (b) for the proposed method and the approach presented in [31] respectively. In stage I, it is observed that with only the primary control activated and using our optimal droop gain settings, both accurate current sharing and a very good bus voltage regulation (the V_{bus} drops to 262 V) can be realized as shown in Fig. 9 (a). On the other hand, though the method proposed in [31] can achieve accurate current sharing using high drop gains at the primary control level, however, the bus voltage drop is very high (the V_{bus} drop to 172.75 V) as shown in Fig. 9 (b). This voltage drop represents about a 36.19 % deviation of the bus voltage from its nominal value. This is not good for loads and may cause instability in the system in case the secondary control fails.

In stage II, both approaches can achieve accurate power sharing and restore the bus voltage to its nominal value simultaneously when the secondary control is activated at t = 0.3 s as shown in Fig. 9 (a) and (b). However, despite the secondary control (SC) being active, the method presented in [31] fails to have good control over the bus voltage when *PMSG-AR$_2$* is assumed to be faulty and temporarily disconnected (i.e., under a source outage (SO)) from the system at t = 0.5 s (i.e., stage III). The bus voltage drops to 233.89 V (representing a voltage drop of about 13.37 % of the nominal value) under the fault condition as shown in Fig. 9 (b). In contrast, our control approach with designed optimal control parameters has excellent control over the bus voltage even under SO (or fault conditions). The bus voltage drops to 266.06 V (representing a voltage drop of only about 1.46 % of the nominal value) as shown in Fig. 9 (a). This clearly shows the superiority of our proposed approach. Therefore, it can be said that the bus voltage regulation performance is significantly affected under the conditions of a source outage (SO) and failure of the secondary control when using the control parameters from [31], while the control parameter obtained using the proposed approach can guarantee desired power sharing and improved bus voltage compensation in different EPS operation conditions.

Furthermore, as shown in Table III, the proposed approach

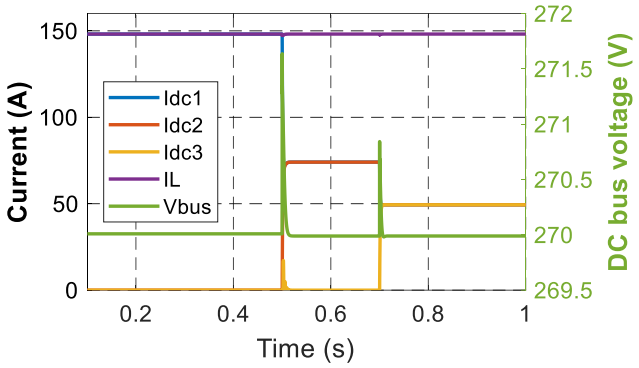

Fig. 10 Simulation results showing the plug-in and plug-out capability of the proposed approach

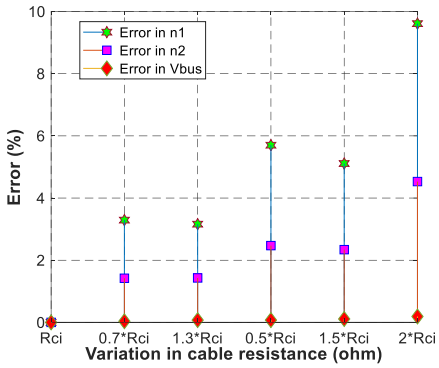

Fig. 11 Effect of variation in cable resistance on current sharing accuracy and bus voltage regulation of the proposed approach.

can reduce the current in the individual branches compared to the method used in [31]. Consequently, the transmission line losses are also reduced. It can therefore be said that the efficiency of the system will be enhanced due to reduced losses in lines as shown in Table III. This can be attributed to the better voltage regulation of the proposed approach compared to the approach used in [31]. The system's stability and overall efficiency will be increased using the proposed control method. Finally, as shown in Fig. 9 (a) and (b), the system is restored to its pre-fault condition immediately after the fault is cleared and the *PMSG-AR*$_2$ is reconnected back to the system at t = 0.7 s.

It is important to state that, in both approaches, if the compensation coefficients are recomputed and immediately updated (in real-time) according to the EPS condition (such as single or multiple sources failures), the bus voltage will be restored to its nominal value. However, our proposed approach may not necessarily require such extra effort since the drop in bus voltage under such conditions is very small and this is a great advantage. A comparison between the proposed approach and some of the existing methods is summarized in TABLE IV. It is observed that, compared to the existing approaches, our proposed approach is robust, easier to implement and can realise good bus voltage regulation under different EPS operation conditions.

3) Case 3: Plug-and-Play Capability

This case study demonstrates the plug-and-play capability of our proposed approach. Here, the surrogate model is trained with data samples obtained under different conditions of the EPS (such as one or two generators failure). To enhance the capability of the proposed strategy, the authors suggest including abnormal operation scenarios in the ANN training to have more dynamic data sets. The data set should be stored in a lookup table to train the corresponding surrogate model [37]. This way, the training sessions will need to be carried out once or less frequently and not whenever the network changes.

The recomputed optimal compensation coefficients are k_{copt} = 1/11.9501 when all three sources are working, k_{copt} = 1/7.9649 when two sources are working, and k_{copt} = 1/3.9798 when only one source is operational. However, irrespective of the number of sources under fault conditions, the other active sources will share the load power demand according to their respective optimal droop gain. Thus, the optimal droop coefficients are unchanged and remain as k_{d1opt} = 1/4.0305, k_{d2opt} = 1/4.5211 and k_{d3opt} = 1/4.2342 for equal load sharing. A CPL of 40 kW is applied at t = 0.1 s during the simulation and the secondary control is also activated.

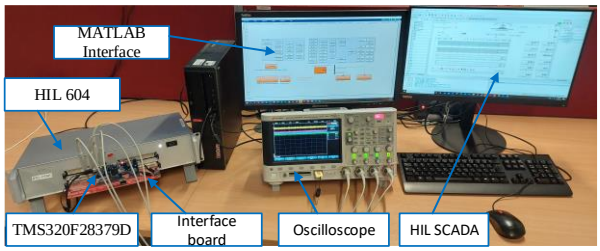

Fig. 12 C-HIL test setup

As shown in Fig. 10, only *PMSG-AR*$_1$ is initially connected to the DC bus, followed by *PMSG-AR*$_2$ and then *PMSG-AR*$_3$. The results obtained show that as the new PMSG-AR system is connected to the DC bus, both accurate power sharing and bus voltage restoration are realized simultaneously.

4) Case 4: Impact of variation in the cable resistance

The line resistance is usually unknown in practice and is considered the major factor that influences the current sharing and voltage deviation in the DC microgrid [12, 23]. Furthermore, it is affected by various factors such as temperature variation, the materials of the transmission cable and their thickness. In this case study, the impact of the variation of the cable resistance on the current sharing and voltage regulation performance of the proposed control method is investigated.

A CPL of 25 kW is applied during the simulation and the optimal droop and compensation coefficients from design example 1 (see section IV-A) are used. The cable resistances are varied by - 30%, 30%, - 50%, 50% and 200% which corresponds to 0.3, 1.3, 0.5, 1.5 and 2 respectively of their initial values shown in Table II. The results obtained are shown in Fig. 11. It can be observed from Fig. 11 that with a variation of -30 %, 30%, -50% and 50% in the cable resistance, the error in the current sharing ratios (n_1 and n_2) from their desired values is mostly around 5 % or less for n_1 and less than 3% for n_2. Some errors in the current sharing are acceptable, especially under light load conditions and provided the sources are working within their capacity [12, 38, 39]. Also, even when the

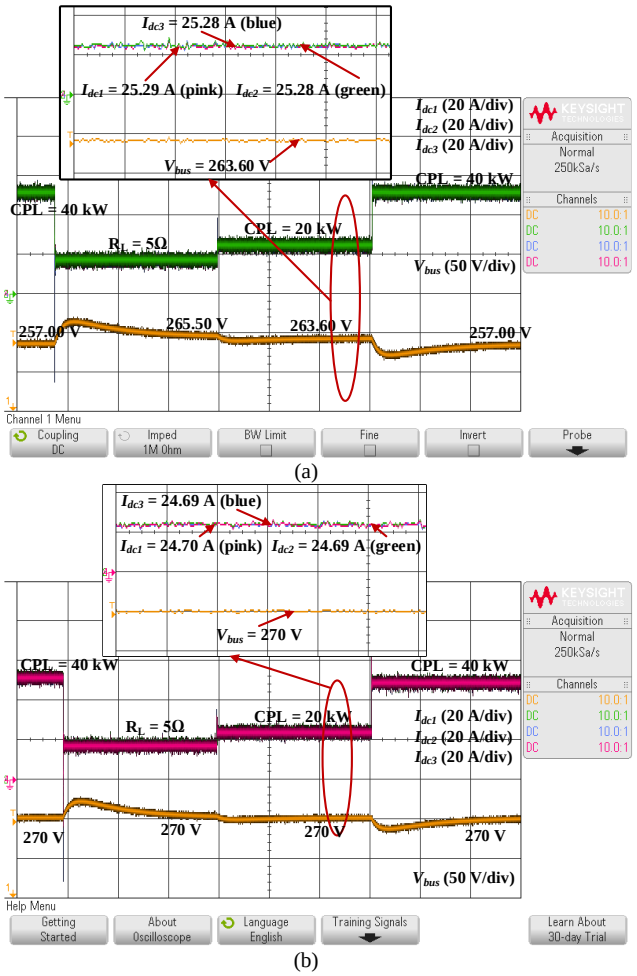

Fig. 13 HIL experimental results for mixed load with equal current sharing and bus voltage regulation using the proposed approach (a) without bus voltage compensation (b) with bus voltage compensation

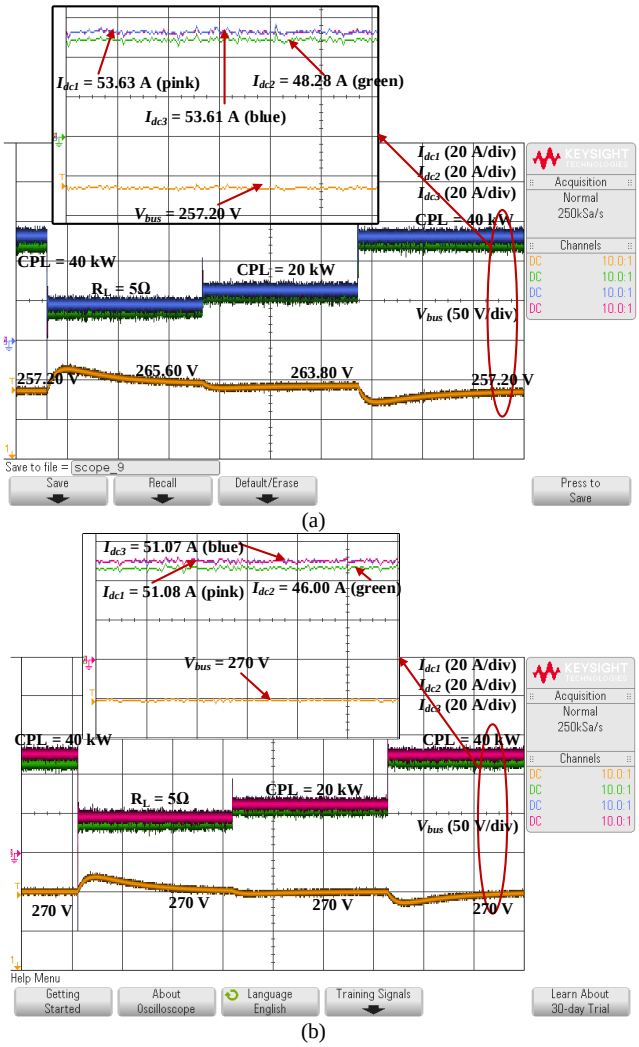

Fig. 14 HIL experimental results for mixed load with unequal current sharing and bus voltage regulation using the proposed approach (a) without bus voltage compensation (b) with bus voltage compensation

cable resistance was doubled, the error in the current sharing ratio n_2 is less than 5 %, while the error in the current sharing ratio n_1 is 9.61%. However, in all the cable resistance variations investigated, the deviation of the bus voltage from its nominal value is less than 0.5%. This verifies the robustness and good steady-state performance of the proposed control approach.

The cable resistance variation test showed that the proposed control method may not yield acceptable control performance for the sharing ratio between converter 1 and 2 (i.e., n_1) for a 200% variation in the cable resistance. In the event of a significant variation in the line resistance, the ANN model will need to be updated accordingly for better current sharing performance of the proposed control method [37].

V. Controller Hardware-in-the-Loop Real-Time Validation

A. *Experimental or Test Setup*

The proposed approach is verified by carrying out a controller hardware-in-the-loop (C-HIL) experiment. The experimental setup is made up of a Typhoon HIL real-time power electronics emulator and a Digital Signal Processor (DSP) controller (i.e., Texas Instrument (TI) DSP TMS320F28379D). The Typhoon HIL real-time emulator is used to emulate the power stage consisting of multiple generators (i.e., the PMSGs), converters and transmission cables and load shown in Fig. 6, while the DSP controller is used to control the emulated system. The DSP controller and the typhoon HIL emulator communicate via an interface board, which facilitates the exchange of data between the two systems. The C-HIL setup is shown in Fig. 12.

The Typhoon HIL real-time emulator used in the experiment is a HIL 604 with 8 processing cores, 64 analogue outputs, 64 digital inputs, and 20 ns PWM resolution combined with 1 µs latency to allow for the most realistic controller test. The power stage is modelled in the typhoon software in real-time and with high fidelity. The TI DSP TMS320F28379D control card with 180-pin used in the experiment is a microcontroller-based system designed for real-time control applications. The Embedded Coder Support Package which is available in MATLAB is used for developing the control algorithms, while the TI Code Composer Studio (CCS) is used for debugging the generated control codes and programming the real DSP control card.

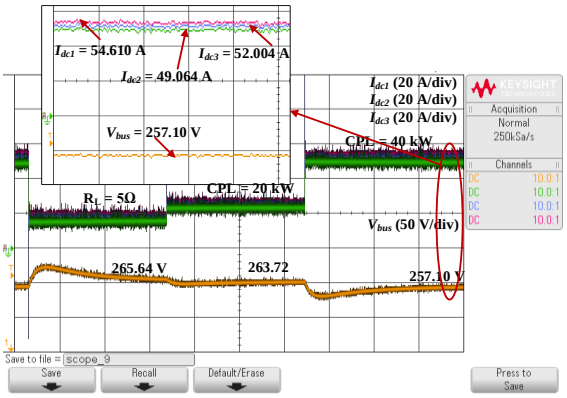

Fig. 15 HIL experimental results for power sharing and bus voltage regulation using the conventional droop control method

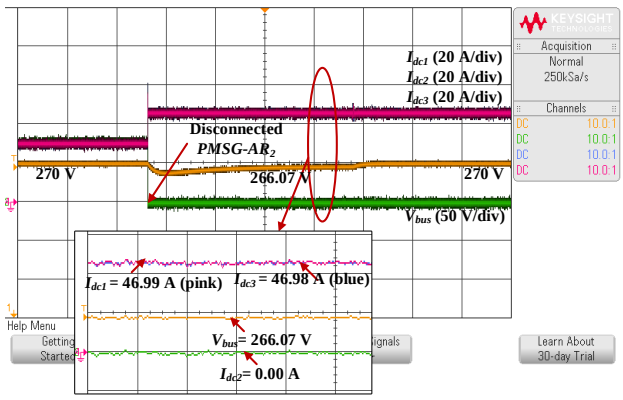

Fig. 16 HIL experimental results for fault scenario with equal current sharing and voltage regulation using the proposed approach

The proposed control strategy as shown in Fig. 6 and the optimized control parameters are implemented in the TI DSP TMS320F28379D control card to generate control signals for the control of the three *PMSG-AR* systems. With the power stage emulated in real-time using the HIL-604 device, the real DSP controller which is the device under test can effectively control the machines and power converters as it would a physical power stage. Based on this and from the controller's point of view, the proposed approach can be said to have been experimentally verified. An oscilloscope was used for results collection. The parameters used for the experiment are the same as those shown in TABLE II.

B. *HIL Results and Analysis*

i. *Case 1: Equal power sharing and bus voltage compensation*

In this case study, our proposed control strategy is demonstrated with a mix of resistive and CPLs changes for equal power sharing and bus voltage regulation as shown in Fig. 13. The results of the experiment using only the optimal droop coefficient settings from the design example 1 and with only the primary control activated is shown in Fig. 13 (a). It can be observed that the optimal droop coefficient can yield equal current sharing among the converters in the desired sharing ratio (with computed n_1 = 1.00, and n_2 = 1.00). However, due to the droop control action, the bus voltage decreases with an increase in the load demand. The normalized bus voltage is computed as V_{bcn} = 0.976 for the 20 kW load bus voltage regulation shown in Fig. 13 (a). Nevertheless, the bus voltage regulation is still within the steady-state acceptable range (i.e., a voltage range of between 250 V to 280 V) for the MEA application [7].

On the other hand, when the optimal droop and compensation coefficient settings (i.e., secondary control activated) from design example 1 are used in this case study, the bus voltage is maintained at its nominal value of 270 V (i.e., $V_{bcndesired}$ =1) despite the load changes as shown in Fig. 13 (b). At the same time, the current is shared equally among the participating converters in the desired sharing ratio (i.e., $n_{1desired}$ = 1 and $n_{2desired}$ = 1). Based on the output current of the converters and bus voltage obtained from the HIL experiment as shown in Fig. 13 (b), the computed current sharing ratios (using (4) and (5)) and normalized bus voltage are n_1 = 0.9996 ≈ 1.00, n_2 = 0.9996 ≈ 1.00, and V_{bcn} = 1.00. The details of the calculations are presented in the appendix. These results show that both equal load sharing and bus voltage compensation can be achieved simultaneously as designed and based on user-defined desired control objectives using the proposed approach. In addition, each of the branch currents is reduced after the bus compensation is implemented as shown in Fig. 13 (b). Thus, it can be said that the proposed secondary control can reduce transmission line losses compared to the conventional droop control method.

ii. *Case 2: Unequal Power Sharing and Bus Voltage Compensation*

In case 2, the flexibility and applicability of the proposed approach are tested for unequal load sharing ($n_{1desired}$ = 0.9 and $n_{2desired}$ = 1) and bus voltage regulation ($V_{bcndesired}$ =1). The load changes in this case study are the same as in case 1. The results of the experiment using only the optimal droop coefficient settings from design example 2 and with only the primary control activated are shown in Fig. 14 (a). It can be observed that the optimal droop coefficient can yield unequal current sharing among the converters in the desired sharing ratio (i.e., with computed n_1 = 0.9 and n_2 = 1.00). However, due to the droop control action, the bus voltage decreases with an increase in the load demand. The normalized bus voltage is computed as V_{bcn} = 0.953 for the 40 kW load bus voltage regulation shown in Fig. 14 (a). Nevertheless, the bus voltage regulation is still within the steady-state acceptable range (i.e., a voltage range of between 250 V to 280 V) for the MEA application [7].

Conversely, by using the optimal droop and compensation coefficient settings from design example 2 and the secondary control activated, the experimental result is shown in Fig. 14 (b). It can be observed that the desired unequal load sharing among the converters and bus voltage restoration is realized simultaneously despite the load fluctuation. The calculated current sharing ratios between the converters and normalized bus voltage in steady-state using the output current of the converters and bus voltage obtained from the HIL experiment as shown in Fig. 14 (b) are n_1 = 0.90, n_2 = 1.00 and V_{bcn} = 1.00 respectively. Thus, yielding the user-defined desired control performance. The details of the calculations are presented in the appendix.

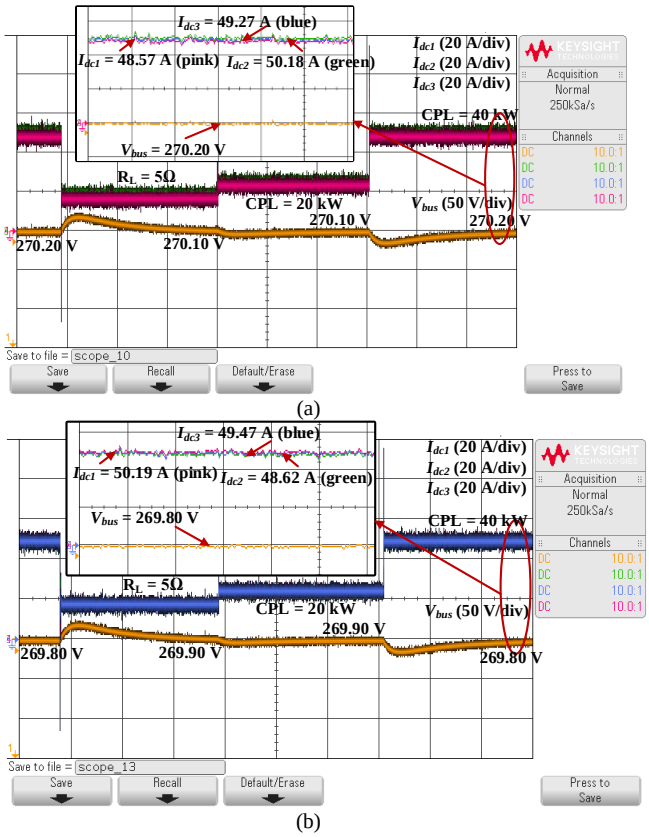

Fig. 17 HIL experimental results for load sharing and bus voltage compensation using the proposed control method, a response to (a) a 30% decrease in the cable parameters (b) a 30% increase in the cable parameters

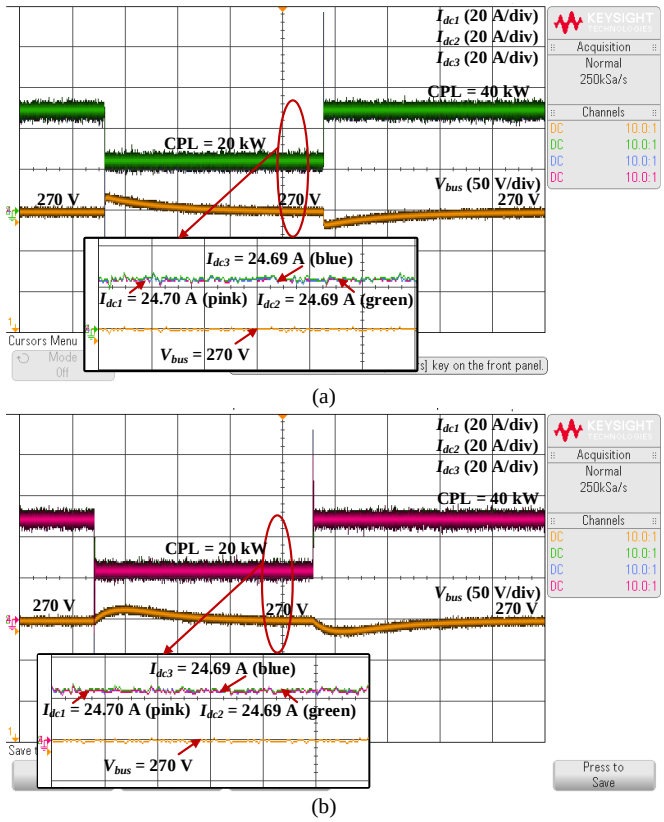

Fig. 18 HIL experimental results for load sharing and bus voltage compensation using the proposed control method, a response to (a) a 30% decrease in the dc-link capacitance (b) a 30% increase in the dc-link capacitance

iii. Case 3: Traditional droop control method

In this case study, the performance of our proposed control strategy is compared with the conventional droop controller. The experiment is carried out using the traditional fixed and identical droop coefficients shown in TABLE II (obtained using the convention droop gain design in (6)). As shown in Fig. 15, the bus voltage regulations are within the acceptable range (i.e., less than 5% of the nominal bus value). However, due to the droop control, the bus voltage regulation will increase with an increase in load demand. On the other hand, the power sharing performance of the droop control method is affected by the unequal distribution line resistance. Based on the output current of the converters shown in Fig. 15, the computed current sharing ratios are n_1 = 0.8984 and n_2 = 0.9523. Thus, representing 10.16% and 4.77% deviations of the current sharing ratio from the desired value. The steps to follow in calculating the current sharing ratios are presented in the appendix.

It can therefore be said that, unlike the conventional droop controller, our proposed control strategy can achieve both accurate power sharing and bus voltage restoration simultaneously. Besides, compared to the conventional fixed and identical droop coefficient, the obtained optimal droop coefficient settings using the proposed design strategy can enhance the current sharing performance of the droop control at the primary control level as shown in Fig. 13 (a).

iv. Case 4: Fault scenario

The robustness of the proposed approach under a source fault condition is demonstrated in the experiment. The optimal coefficient settings from design example 1 are used here. A CPL of 25 kW is used in the experiment and the secondary control is also implemented. The experimental result is shown in Fig. 16.

As shown in Fig. 16, it can be observed that the three parallel-connected converters are initially operating together and shared the load current equally as desired. Furthermore, the bus voltage is regulated at its reference value of 270 V. When *PMSG-AR*$_2$ is disconnected from the system (assumed to be under fault), the current demand is shared equally as desired by the two remaining converters after the loss of converter 2. However, the bus voltage experienced a little drop to about 266.07 V during the fault duration (representing a voltage drop of 1.42 % of the nominal bus value). However, immediately after the optimal compensation coefficient k_{copt} is updated (new k_{copt} = 1/7.9649) based on the EPS condition, the bus voltage is restored to its nominal value. Hence, this demonstrates the robustness and good fault tolerance capability of the proposed approach.

v. Case 5: Parameter uncertainty

In this case study, the robustness of the proposed control approach to parameter changes in the power system is assessed, this is particularly important when there are no parameter estimation algorithms to adapt to the changes. Some of the parameters that could change during the system operation due to operating temperature or other factors include the cable

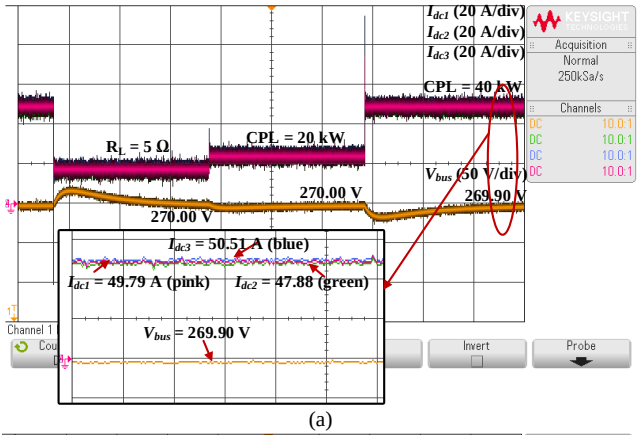

(a)

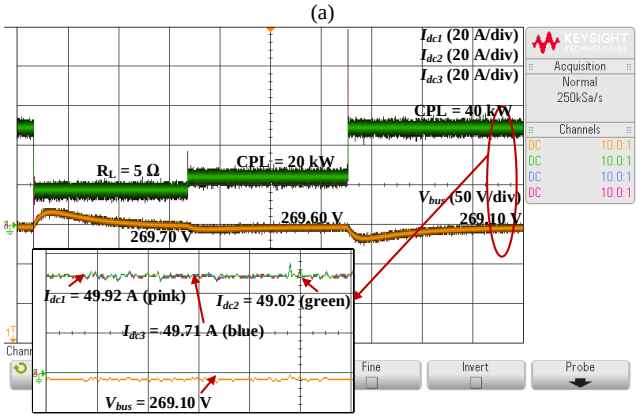

(b)

Fig. 19 HIL experimental results for current sharing and bus voltage compensation, considering opposite changes to the parameters in the different cables. The response to a +/- 30% variation is shown for both (a) the proposed method and (b) the method described in [31].

impedance (i.e., L_{ci} and R_{ci}), DC-link capacitance C_b, stator winding inductance and resistance (i.e., $L_{d,q}$ and R_s) and the machine flux ψ_m. However, due to space limitations, we are only going to assess the variation in the cable impedance and DC-link capacitance in this article. The optimal coefficient settings from design example 1 are used in this case study.

To demonstrate the variation in the cable impedance in the experiment, the conductor's parasitic inductance and resistance are varied by - 30% and 30% of their nominal values shown in TABLE II. The experimental result is shown in Fig. 17 (a) and (b) respectively. Based on the output current of the converters and voltage regulation shown in Fig. 17 (a), the computed current sharing ratios and normalized bus voltage are n_1 = 1.033, n_2 = 1.014, and V_{bcn} = 1.00074 respectively. These correspond to 3.30%, and 1.40% deviations of the current sharing ratios from the desired value. The bus voltage deviation from its nominal value is only 0.074 %. The steps to follow in calculating the current sharing ratios and normalized bus voltage are presented in the appendix.

Similarly, based on the output current of the converters and voltage regulation shown in Fig. 17 (b), the computed current sharing ratios and normalized bus voltage are n_1 = 0.9687, n_2 = 0.9857, and V_{bcn} = 0.9993 respectively. These correspond to 3.13 %, and 1.43 % deviations of the current sharing ratios from the desired value. The bus voltage deviation from its nominal value is only 0.074 %. Though the deviation in the distribution line impedance from their nominal value affects the designed and desired control performance as shown in Fig. 17 (a) and (b), it is observed that the proposed control method is still able to guarantee a significant reduction in the power sharing error and maintain the bus voltage near its nominal value despite the variation in the line impedance. Thus, the proposed approach can be said to be robust to a variation in the distribution line impedance.

Also, the dc-link capacitance C_b is varied by - 30% and 30% of its nominal value shown in Table II. The 30% decrease and increase in the dc-link capacitance did not affect the designed and desired control performance of the proposed control approach as shown in Fig. 18 (a) and (b) respectively. The 30% reduction in the dc-link capacitance mainly causes some small oscillations in the output current of the converters as shown in Fig. 18 (a), however, the control is still stable.

Based on the results shown in Fig. 17 and 18, it can be said that the proposed control approach is robust and will perform well under system parameter uncertainty.

vi. Case 6: Comparison with the Method in [31]under parameter uncertainty

In this case study, the steady-state control performance of the proposed method is further validated and compared to the approach proposed in [31] under parameter uncertainty by considering opposite changes to the parameters in the different cables. To that end, the line impedance parameters in cables 1 and 3 are decreased by 30% while the line impedance in cable 2 is increased by 30%. In our control scheme, the droop and compensation coefficients obtained from design example 1 are used (i.e., k_{d1opt} = 1/4.0305, k_{d2opt} = 1/4.5211, k_{d3opt} = 1/4.2342, and k_{copt} = 1/11.9501). For the scheme described in [31], the parameters are $k_{d1} = k_{d2} = k_{d3} = 2$, and $k_c = 2/3$. The experimental results are shown in Fig. 19.

Based on the output current of the converters and voltage regulation shown in Fig. 19 (a), the computed current sharing ratios and normalized bus voltage are n_1 = 0.9616, n_2 = 1.0145, and V_{bcn} = 0.9996 respectively for our proposed method. These values correspond to a deviation of 3.84% and 1.45% in the current sharing ratios from the desired value. Furthermore, the bus voltage deviation from its nominal value is merely 0.037%. On the other hand, according to the output current of the converters and voltage regulation depicted in Fig. 19 (b), the calculated current sharing ratios and normalized bus voltage for the method proposed in [31] are as follows: n_1 = 0.9820, n_2 = 0.9958, and V_{bcn} = 0.9967, respectively. These values indicate that there is a deviation of 1.80% and 0.42% in the current sharing ratios from the desired value. Additionally, the bus voltage shows a deviation of only 0.33% from its nominal value.

Based on the presented results, it is evident that both approaches are influenced by variations in the line impedance parameter, affecting their control performance. The approach proposed in [31], which involves setting high droop gains for the converters, as expected demonstrates better adaptability to changes in the line impedance parameter in terms of current sharing. However, our detailed case study comparison between the proposed method and the approach in [31] (see case 2 under section IV-B) reveals that employing large droop gains at the primary control level has certain drawbacks. One of the drawbacks is inadequate voltage regulation, particularly noticeable during secondary control failure and under source

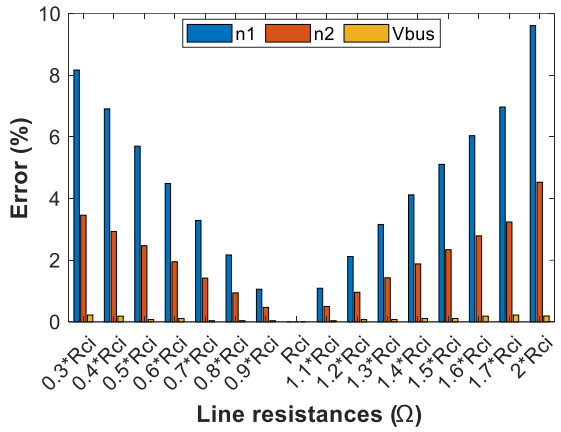

Fig. 20 Figure 20 provides a summary of the deviations in current sharing ratios and voltage regulation resulting from the variations between the line resistances used in data generation and the HIL experimental setup.

fault conditions. Such scenarios can result in unstable voltage levels, which are unfavourable for practical applications, especially for loads onboard the MEA. Furthermore, setting large droop gains can lead to increased transmission line losses under such scenarios due to the voltage drops, reducing the overall system efficiency. In contrast, our proposed approach offers a combination of satisfactory power sharing and improved voltage regulation performance across various operating conditions of the EPS. This capability to maintain acceptable power sharing while ensuring stable voltage regulation represents a significant contribution to the proposed control method.

vii. Case 7: Analysis of the impact of variation between simulation and experimental parameters

The purpose of this case study is to analyze the impact of parameter variations between the simulation model used for generating training data and the HIL experimental setup on the control performance. It aims to determine the acceptable differences in parameters while maintaining satisfactory control performance. Additionally, practical conditions may not perfectly align with the training data, leading to discrepancies between expected and actual performance. While the system comprises multiple parameters, this analysis specifically focuses on the variation in transmission line resistance. The line resistance is considered the primary parameter influencing the control performance of the system [12].

In this case study, we examine various adjustments to the line resistance parameters in the HIL experiment. These adjustments involve different percentages of variation, such as -/+ 10%, -/+ 20%, -/+ 30%, and so on. Each percentage corresponds to a specific range of values, for example, 0.9/1.1, 0.8/1.2, and 0.7/1.3, respectively, relative to the line resistance values used in the simulation model for generating the training data (referred to as R_{ci} in Table II). To illustrate this concept, refer to Fig. 20, which provides a visual representation of how the different variations relate to the line resistance values employed in the simulation model. By considering these variations, we can assess the impact of changes in line resistance on the system's performance and evaluate the robustness of the proposed approach.

As depicted in Fig. 20, if the line resistance values used in the simulation model for generating the training data match those in the HIL experiment, the desired and designed control performance is achieved with perfect accuracy. Furthermore, it is important to acknowledge that changes in the interconnecting cable resistance can have an impact on the distribution of current among the various sources. These changes lead to deviations from the intended current sharing ratios. It is worth noting that the observed deviations in the current sharing ratios are within tolerable limits [12], being around 5% for n_1 and below 3% for n_2, for a variation of up to -/+ 50%. As shown in Fig. 20, for a variation beyond -/+ 50%, the steady-state control performance becomes deteriorated, especially for the current ratio n_1. Nevertheless, across the examined variations, the maximum deviation in the current sharing ratios is less than 10% for n_1 and less than 5% for n_2, for a 200% variation in the cable resistance parameter. On the other hand, the bus voltage is well-regulated despite the different variations in the line resistance.

VI. Conclusion

In this paper, a novel design strategy for the computation of the optimal power sharing and bus voltage compensation coefficients for the islanded DC MG of the MEA EPS is presented. The proposed design strategy utilized an ANN-based surrogate model for the computation of the optimal droop and bus voltage compensation coefficient settings. The performance of the MEA EPS distribution network with the optimized control parameters obtained from the proposed approach is compared with the control parameters obtained from the approach proposed in [31]. The simulation results showed that the power sharing and bus voltage regulation performance of the MEA EPS distribution network using the control parameters obtained from the proposed approach is better than with the control parameters obtained from the approach proposed in [31] in different conditions of the EPS. Different C-HIL experimental case studies have been carried out to demonstrate the effectiveness of the proposed approach. The proposed approach does not require extra digital communication lines and controllers in its implementation. In the future, we intend to apply the proposed design strategy to other MG topologies for terrestrial applications.

Appendix

The actual math calculation and evidence on how the values of the current sharing ratios and normalized bus voltage in the validation section are obtained are elaborated here.

Case 1: Equal power sharing and bus voltage compensation

Based on the output current of the converters and bus voltage obtained from the HIL experiment as shown in Fig. 13 (b), the current sharing ratios and normalized bus voltage can be calculated as follows.

By substituting the output current of the converters, optimal droop gain settings from design example 1 (see section IV-A) and DC cable parameters shown in Table II into equations (4) and (5), the current sharing ratios can be calculated as:

$$n_1 = \frac{I_{dc2}}{I_{dc1}} = \frac{k_{d1} + R_{c1}}{k_{d2} + R_{c2}} \Leftrightarrow \frac{24.69}{24.70} = \frac{\frac{1}{4.0305} + 0.003}{\frac{1}{4.5211} + 0.03} = \frac{0.2511}{0.2512} = 0.9996 \approx 1.00$$

$$n_2 = \frac{I_{dc3}}{I_{dc1}} = \frac{k_{d1} + R_{c1}}{k_{d3} + R_{c3}} \Leftrightarrow \frac{24.69}{24.70} = \frac{\frac{1}{4.0305} + 0.003}{\frac{1}{4.2342} + 0.015} = \frac{0.2511}{0.2512} = 0.9996 \approx 1.00$$

The normalized bus voltage is obtained as $V_{bcn} = \frac{V_{bus}}{270} = \frac{270}{270} = 1$.

Case 2: Unequal Power Sharing and Bus voltage compensation

Based on the output current of the converters and bus voltage obtained from the HIL experiment as shown in Fig. 14 (b), the current sharing ratios and normalized bus voltage can be calculated as follows.

By substituting the output current of the converters, optimal droop gain settings from design example 2 and DC cable parameters in Table II into equations (4) and (5), the current sharing ratios can be calculated as:

$$n_1 = \frac{I_{dc2}}{I_{dc1}} = \frac{k_{d1} + R_{c1}}{k_{d2} + R_{c2}} \Leftrightarrow \frac{46.00}{51.08} = \frac{\frac{1}{4.2434} + 0.003}{\frac{1}{4.2540} + 0.03} = \frac{0.2387}{0.2651} = 0.90$$

$$n_2 = \frac{I_{dc3}}{I_{dc1}} = \frac{k_{d1} + R_{c1}}{k_{d3} + R_{c3}} \Leftrightarrow \frac{51.07}{51.08} = \frac{\frac{1}{4.2434} + 0.003}{\frac{1}{4.4698} + 0.015} = \frac{0.2387}{0.2387} = 1.00$$

The normalized bus voltage is obtained as $V_{bcn} = \frac{V_{bus}}{270} = \frac{270}{270} = 1$.

The same steps as shown in case 1 and case 2 are followed for all other cases to compute the current sharing ratios and normalized bus voltage.

REFERENCES

[1] Q. Xu, X. Hu, P. Wang, J. Xiao, P. Tu, C. Wen and M. Y. Lee, "A decentralized dynamic power sharing strategy for hybrid energy storage system in autonomous DC Microgrid," *IEEE Transactions on industrial electronics*, vol. 64, no. 7, pp. 5930-5941, July 2017.

[2] J. A. Rosero, J. A. Ortega, E. Aldabas and L. A. R. L. Romeral, "Moving towards a more electric aircraft," *IEEE Aerospace and Electronic Systems Magazine*, vol. 22, no. 3, pp. 3-9, 2007.

[3] P. Wheeler and S. Bozhko, "The more electric aircraft: Technology and challenges," *IEEE Electrification Magazine*, vol. 2, no. 4, pp. 6-12, 2014.

[4] F. Gao, S. Bozhko, A. Costabeber, G. Asher and P. Wheeler, "Control design and voltage stability analysis of a droop-controlled electrical power system for more electric aircraft," IEEE Transactions on Industrial Electronics, vol. 64, no. 12, pp. 9271-9281, December 2017.

[5] J. M. Guerrero, J. C. Vasquez, J. Matas, L. G. De Vicuña and M. Castilla, "Hierarchical control of droop-controlled AC and DC microgrids—A general approach toward standardization," *IEEE Transactions on industrial electronics*, vol. 58, no. 1, pp. 158-172, January 2011.

[6] B. Wang, G. Vakil, Y. Liu, T. Yang, Z. Zhang and C. Gerada, "Optimization and analysis of a high power density and fault tolerant starter–generator for aircraft application," *Energies*, vol. 14, no. 1:113, pp. 1-16, 2021.

[7] MIL-STD-704F, " Department of Defense Interface Standard. Aircraft Electric Power Characteristics," [Online]. Available: http://everyspec.com/MIL-STD/MIL-STD-0700-0799/MIL-STD-704F_1083/. [Accessed 8 August 2019].

[8] "DO-160E Environmental Conditions and Test Procedures for Airborne Equipment," RTCA Standard, 2004.

[9] Y. Han, X. Ning, P. Yang and L. Xu, "Review of power sharing, voltage restoration and stabilization techniques in hierarchical controlled DC microgrids," *IEEE Access*, vol. 7, pp. 149202-149223, 2019.

[10] J. M. Guerrero, M. Chandorkar, T. L. Lee and P. C. Loh, "Advanced control architectures for intelligent microgrids—Part I: Decentralized and hierarchical control," *IEEE Transactions on Industrial Electronics*, vol. 60, no. 4, pp. 1254-1262, April 2013.

[11] F. Gao, R. Kang, J. Cao and T. Yang, "Primary and secondary control in DC microgrids: a review," *Journal of Modern Power Systems and Clean Energy*, vol. 7, no. 2, pp. 227-242, 2019.

[12] S. Anand, B. G. Fernandes and J. Guerrero, "Distributed control to ensure proportional load sharing and improve voltage regulation in low-voltage DC microgrids," *IEEE Transactions on power electronics*, vol. 28, no. 4, pp. 1900-1913, April 2013.

[13] X. Lu, J. M. Guerrero, K. Sun and J. C. Vasquez, " An improved droop control method for dc microgrids based on low bandwidth communication with dc bus voltage restoration and enhanced current sharing accuracy," *IEEE Transactions on Power Electronic*, vol. 29, no. 4, pp. 1800-1812, April 2014.

[14] V. Nasirian, S. Moayedi, A. Davoudi and F. L. Lewis, "Distributed cooperative control of DC microgrids," *IEEE Transactions on Power Electronics*, vol. 30, no. 4, pp. 2288-2303, April 2015.

[15] N. Yang, D. Paire, F. Gao, A. Miraoui and W. Liu, "Compensation of droop control using common load condition in DC microgrids to improve voltage regulation and load sharing," *International Journal of Electrical Power & Energy Systems*, vol. 64, pp. 752-760, 2015.

[16] P. H. Huang, Liu, P. C., W. Xiao and M. S. El Moursi, "A novel droop-based average voltage sharing control strategy for DC microgrids," *IEEE Transactions on Smart Grid*, vol. 6, no. 3, pp. 1096-1106, May 2015.

[17] P. Prabhakaran, Y. Goyal and V. Agarwal, "A novel communication-based average voltage regulation scheme for a droop controlled DC microgrid," *IEEE Transactions on Smart Grid*, vol. 10, no. 2, pp. 1250-1258, March 2019.

[18] P. Wang, X. Lu, X. Yang, W. Wang and D. Xu, "An improved distributed secondary control method for DC microgrids with enhanced dynamic current sharing performance," *IEEE Transactions on Power Electronics*, vol. 31, no. 9, pp. 6658-6673, September 2016.

[19] F. Gao, S. Bozhko and P. Wheeler, "An enhanced secondary control approach for voltage restoration in the DC distribution system," *SAE Technical Paper*, No. 2016-01-1985, 2016.

[20] F. Guo, Q. Xu, C. Wen, L. Wang and P. Wang, " Distributed secondary control for power allocation and voltage restoration in islanded DC microgrids," *IEEE Transactions on Sustainable Energy*, vol. 9, no. 4, pp. 1857-1869, October 2018.

[21] L. Xing, Y. Mishra, F. Guo, P. Lin, Y. Yang, G. Ledwich and Y. C. Tian, "Distributed secondary control for current sharing and voltage restoration in DC microgrid," *IEEE Transactions on Smart Grid*, vol. 11, no. 3, pp. 2487-2497, May 2020.

[22] N. Ghanbari and S. Bhattacharya, "Adaptive droop control method for suppressing circulating currents in dc microgrids," *IEEE Open Access Journal of Power and Energy*, vol. 7, pp. 100-110, 2020.

[23] N. Mohammed, L. Callegaro, M. Ciobotaru and J. M. Guerrero, "Accurate power sharing for islanded DC microgrids considering mismatched feeder resistances," *Applied Energy*, vol. 340, no. 121060, 2023.

[24] J. Chen and Q. Song, "A decentralized dynamic load power allocation strategy for fuel cell/supercapacitor-based APU of large more electric vehicles," *IEEE Transactions on Industrial Electronics*, vol. 66, no. 2, pp. 865-875, Feb. 2019.

[25] C. Deng, F. Guo, C. Wen, D. Yue and Y. Wang, "Distributed resilient secondary control for DC microgrids against heterogeneous communication delays and DoS attacks," *IEEE Transactions on Industrial Electronics*, vol. 69, no. 11, pp. 11560-11568, November 2022.

[26] M. S. Sadabadi, N. Mijatovic and T. Dragičević, "A Robust Cooperative Distributed Secondary Control Strategy for DC Microgrids with Fewer Communication Requirements," *IEEE Transactions on Power Electronics*, 2022.

[27] A. Tah and D. Das, " An enhanced droop control method for accurate load sharing and voltage improvement of isolated and interconnected DC microgrids," *IEEE Transactions on Sustainable Energy*, vol. 7, no. 3, pp. 1194-1204, 2016.

[28] S. Peyghami, H. Mokhtari, P. C. Loh, P. Davari and F. Blaabjerg, "Distributed primary and secondary power sharing in a droop-controlled

LVDC microgrid with merged AC and DC characteristics," *IEEE Transactions on Smart Grid*, vol. 9, no. 3, pp. 2284-2294, May 2018.
[29] W. Jiang, J. Zhao, K. Qu, L. Mao, Y. Zhu and H. Liu, "An Enhanced Drop Control Method for DC Microgrids with Accurate Current Sharing and DC Bus Voltage Restoration," in *2019 4th International Conference on Intelligent Green Building and Smart Grid (IGBSG)*, Hubei, China, 2019.
[30] S. Peyghami, H. Mokhtari and F. Blaabjerg, "Decentralized load sharing in a low-voltage direct current microgrid with an adaptive droop approach based on a superimposed frequency," *IEEE Journal of Emerging and Selected Topics in Power Electronics*, vol. 5, no. 3, pp. 1205-1215, September 2017.
[31] F. Gao, S. Bozhko, G. Asher, P. Wheeler and C. Patel, "An Improved Voltage Compensation Approach in a Droop-Controlled DC Power System for the More Electric Aircraft," *IEEE Transactions on Power Electronics*, vol. 31, no. 10, pp. 7369 - 7383, 2016.
[32] F. Cingoz, A. Elrayyah and Y. Sozer, "Optimized settings of droop parameters using stochastic load modelling for effective DC microgrids operation," *IEEE Transactions on Industry Applications*, vol. 53, no. 2, pp. 1358-1371, March-April 2017.
[33] S. Zhao, F. Blaabjerg and H. Wang, "An overview of artificial intelligence applications for power electronics," *IEEE Transactions on Power Electronics*, vol. 36, no. 4, pp. 4633 - 4658, 2021.
[34] S. Skansi, *Introduction to Deep Learning: from logical calculus to artificial intelligence*, Springer, 2018.
[35] T. Guillod, P. Papamanolis and J. W. Kolar, "Artificial neural network (ANN) based fast and accurate inductor modelling and design," *IEEE Open Journal of Power Electronics*, vol. 1, pp. 284-299, July 2020.
[36] F. Gao, S. Bozhko, A. Costabeber, C. Patel, P. Wheeler, C. I. Hill and G. Asher, "Comparative stability analysis of droop control approaches in voltage-source-converter-based DC microgrids," *IEEE Transactions on Power Electronics*, vol. 32, no. 3, pp. 2395 - 2415, March 2017.
[37] P. R. Bana and M. Amin, "Control for Grid-Connected VSC With Improved Damping Based on Physics-Informed Neural Network," *IEEE Journal of Emerging and Selected Topics in Industrial Electronics*, March 2023.
[38] S. Sharma, V. M. Iyer, S. Bhattacharya and K. Zou, "New Mesh Configurations with Decentralized Droop Control Method for DC Microgrids," *IEEE Transactions on Industrial Electronics*, pp. 1 - 10, February 2023.
[39] F. Chen, R. Burgos, D. Boroyevich, J. C. Vasquez and J. M. Guerrero, "Investigation of nonlinear droop control in DC power distribution systems: Load sharing, voltage regulation, efficiency, and stability," *IEEE Transactions on Power Electronics*, vol. 34, no. 10, pp. 9404 - 9421, October 2019.

Habibu Hussaini was born in Minna, Nigeria. He received his B.Eng. degree in Electrical and Computer Engineering from the Federal University of Technology, Minna, Nigeria in 2010. He obtained his MSc. in Energy and Sustainability with Electrical Power Engineering from the University of Southampton, the United Kingdom in 2015. He is currently studying for his Ph.D. in Electrical and Electronics Engineering at the University of Nottingham, United Kingdom.

His research interests include aircraft electrical power systems, artificial intelligence-based design, control and parameter identification, and power electronics and control.

Tao Yang (Senior Member, IEEE) received the Ph.D. degree in electrical engineering from the University of Nottingham, Nottingham, U.K., in 2013.

Since then, he has been a Researcher with the Power Electronics, Machines and Control Group, University of Nottingham, where he became an Assistant Professor in 2016 and an Associate Professor in 2019. His research interests include high-speed electric motor drive control, power electronic conversion, and electrical system design and optimization for more-electric/hybrid/all-electric aircraft applications

Dr. Yang is a Fellow of IET and Higher Education Academy, and an Associate Editor for the IEEE Transactions on Transportation Electrification and Chinese Journal of Aeronautics.

Ge Bai (Student Member, IEEE) received the M.Sc. degree from the University of Nottingham, UK, in 2021. She is currently working toward the Ph.D. degree in Electrical and Electronic Engineering with the Power Electronics, Machines, and Control Group, University of Nottingham, UK.

Her research interests include high-speed machine drives, advanced integrated power generation center for more-electric aircraft, and dc microgrid stability.

Matías Urrutia was born in Santiago, Chile. He received the Electrical Engineer degree and MSc. In Electrical Engineering from Federico Santa Maria Technical University (UTFSM) in 2017. In 2022, Mr. Urrutia obtained a dual-degree PhD in Electrical and Electronic Engineering from the University of Chile and the University of Nottingham. He was a part-time lecturer at the UTFSM Electrical Engineering Department from 2018 to 2021. From May 2021 to March 2023, he worked as a Research Fellow in the PEMC group of the University of Nottingham. Since April 2023, he has been a Senior Power Electronics Engineer at Sprint Electric Ltd, United Kingdom.

His main interests are Modular Multilevel Converters, Matrix Converters, Model predictive Control and modern FPGA-based digital control schemes for power electronics applications.

Serhiy Bozhko (Senior Member, IEEE) received the M.Sc. and Ph.D. degrees in electromechanical systems from the National Technical University of Ukraine, Kyiv, Ukraine, in 1987 and 1994, respectively. Since 2000, he has been with the Power Electronics, Machines and Controls Research Group, University of Nottingham, Nottingham, U.K., where he is currently a Professor of aircraft electric power systems and the Director of the Institute for Aerospace Technology. He is leading several EU- and industry funded projects in the area of aircraft electric power systems, including power generation, distribution and conversion, power quality, control and stability issues, power management and optimization, and advanced modeling and simulation methods.